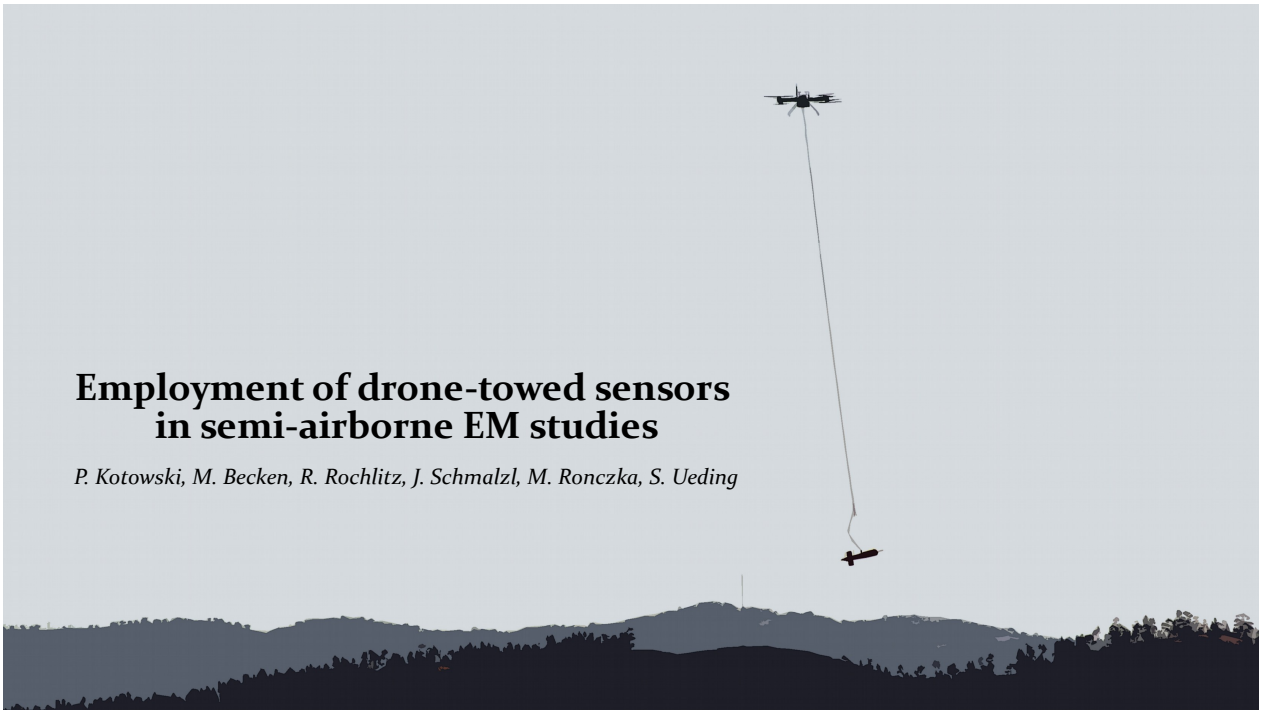

Preface: drone-borne data

Benefits and challenges in drone-based surveys:

- advantages of airborne data acquisition
- high agility during flight
- personnel and operating expenses

- payload and flight duration
- visibility and weather conditions
- **system-related EM noise**

Desired field information is preserved

when

- *no additional superposition (anthropogenic noise, vehicle noise, motion noise, device currents, ..)*
- *no field direction misalignment*
- *signal > sensor sensitivity*
- *no loss of information due to logging*

Preface: drone-borne data

Fig. 1: Survey site in Merfeld (Germany, 2021). The EM transmitter is located about 1 km to the south.

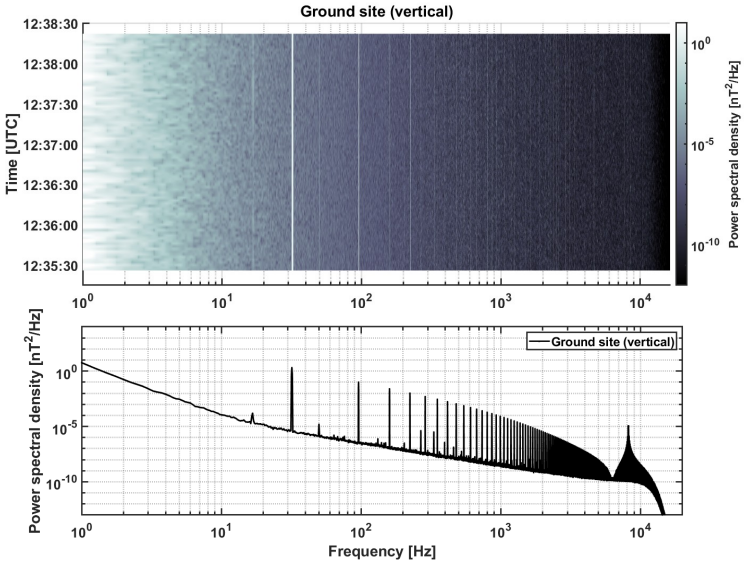

Fig. 2: Field spectra of the ground site. Shown is a time-dependent (top) and an averaged (bottom) spectrum of the vertical magnetic flux density.

Preface: drone-borne data

Fig. 1: Survey site in Merfeld (Germany, 2021). The EM transmitter is located about 1 km to the south.

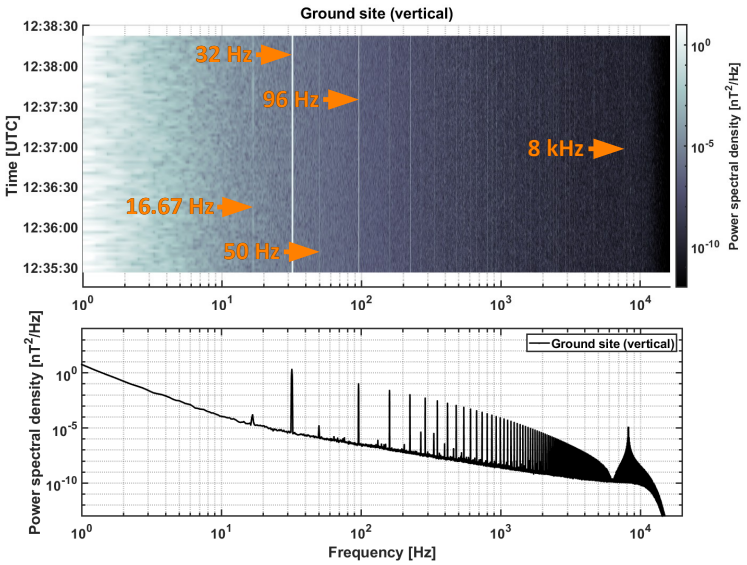

Fig. 2: Field spectra of the ground site. Shown is a time-dependent (top) and an averaged (bottom) spectrum of the vertical magnetic flux density.

Preface: drone-borne data

Fig. 1: Survey site in Merfeld (Germany, 2021). The EM transmitter is located about 1 km to the south.

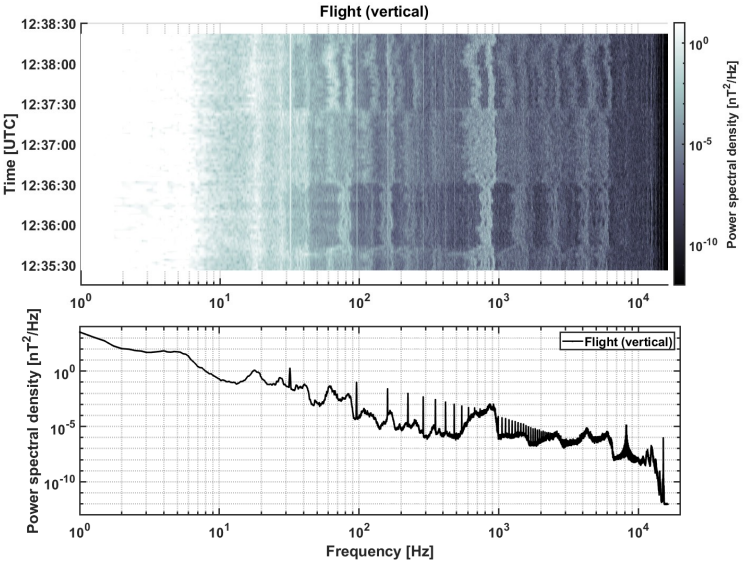

Fig. 3: Field spectra during flight. Shown is a time-dependent (top) and an averaged (bottom) spectrum of the vertical magnetic flux density.

Preface: drone-borne data

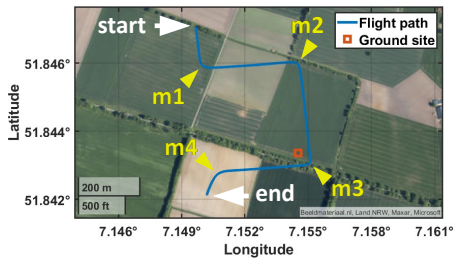

Fig. 1: Survey site in Merfeld (Germany, 2021). The EM transmitter is located about 1 km to the south.

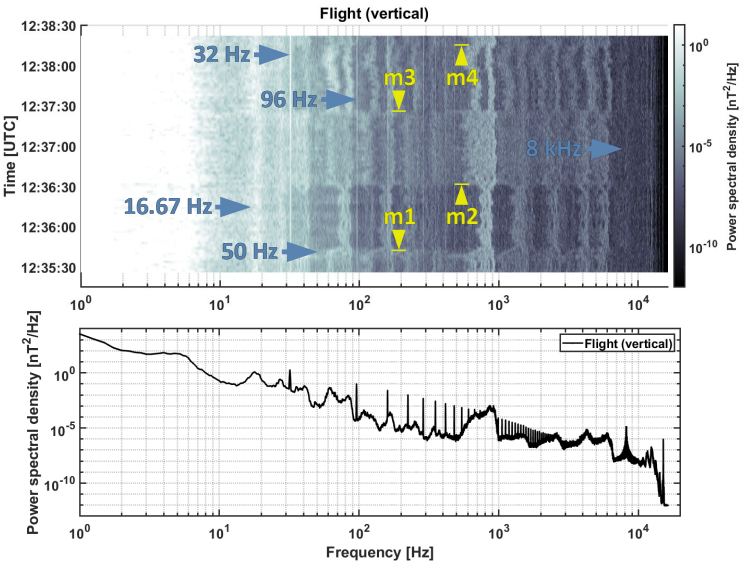

Fig. 3: Field spectra during flight. Shown is a time-dependent (top) and an averaged (bottom) spectrum of the vertical magnetic flux density.

Outline

I: The semi-airborne EM technique

II: Employed sensor platforms

III: Data consistency of differing sensors

IV: System-related EM noise

V: Conclusion & Outlook

WWU MÜNSTER

p. 6/18

The semi-airborne EM technique

- **Transmitters:**
  loop configurations, grounded dipoles
- **Operating frequencies:**
  1 Hz to 10 kHz
- **Processing:**
  frequency domain
- **Exploration depths:**
  < 1 km

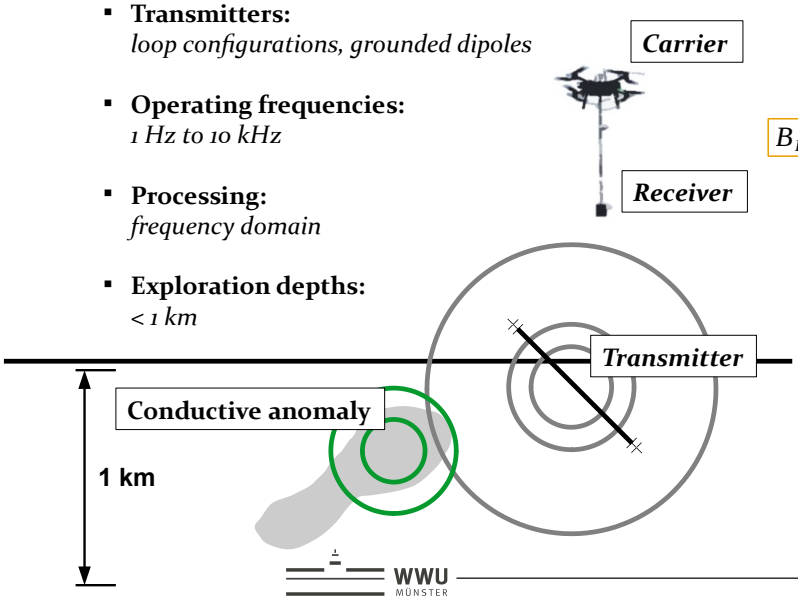

- **Field response (TD)**

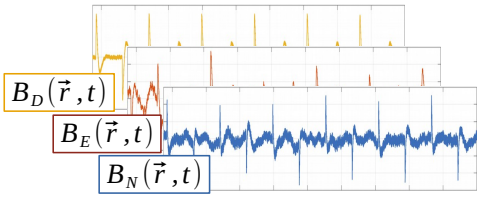

- **Injected current (TD)**

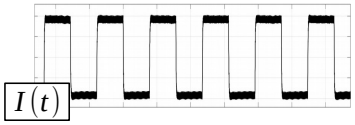

WWU MÜNSTER

p. 7/18

The semi-airborne EM technique

- **Transmitters:**
  loop configurations, grounded dipoles
- **Operating frequencies:**
  1 Hz to 10 kHz
- **Processing:**
  frequency domain
- **Exploration depths:**
  < 1 km

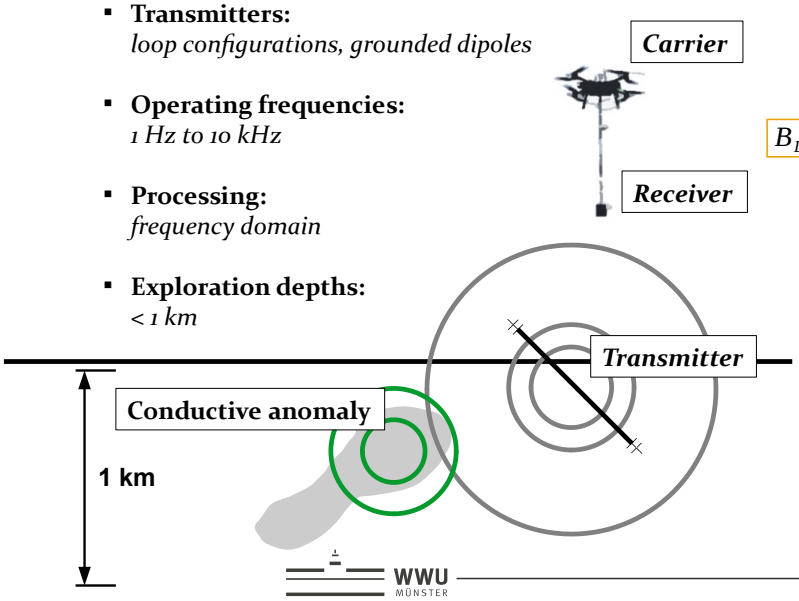

- **Field response (FD)**

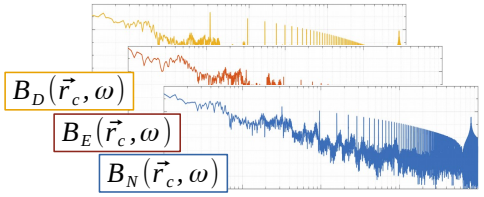

- **Injected current (FD)**

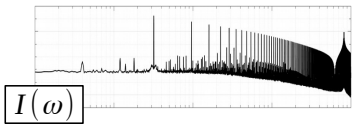

- **Transfer function (FD)**

$$\vec{T}(\vec{r},\omega) = \vec{B}(\vec{r},\omega)I^{-1}(\omega)$$

WWU MÜNSTER

p. 8/18

Employed sensor platforms

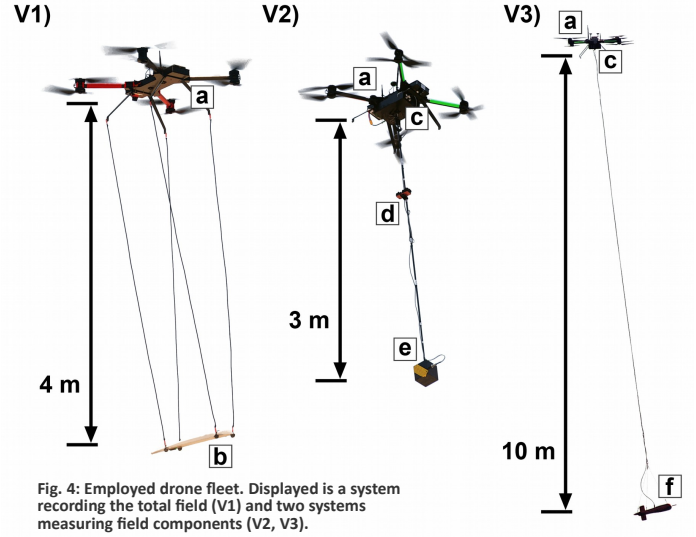

Fig. 4: Employed drone fleet. Displayed is a system recording the total field (V1) and two systems measuring field components (V2, V3).

V1
Scalar total field magnetometer (OPM)

- Frequency range:
  1 to 250 Hz

V2 and V3
Vector induction coil triple (IC)

- Frequency range:
  30 Hz to 6 kHz

WWU MÜNSTER

p. 9/18

Employed sensor platforms

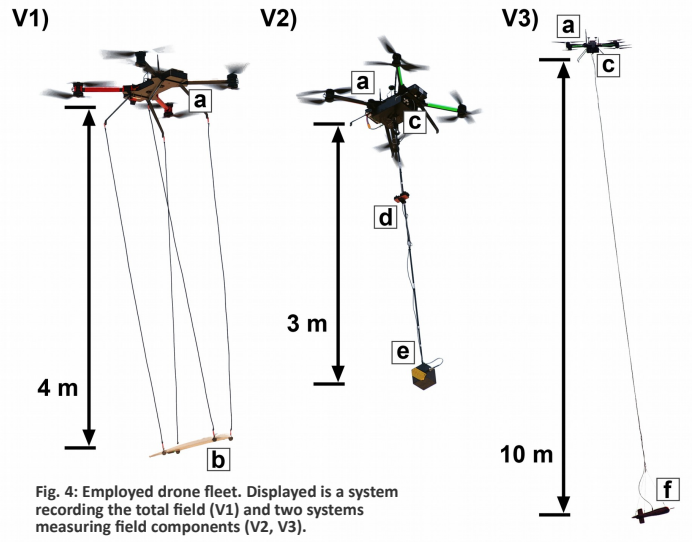

Fig. 4: Employed drone fleet. Displayed is a system recording the total field (V1) and two systems measuring field components (V2, V3).

[a]: Carrier (uncrewed aircraft)
Battery-powered octocopter

[b]: Sensor (scalar magnetometer)
Optically pumped magnetometer (OPM)

[c]: Data logger
24/32 Bit A/D converter

[d]: Sensor (spatial navigation)
Inertial measurement unit (IMU)

[e]: Sensor (vector magnetometer)
Induction coil (IC) triple

[f]: Sensor casing (vector magnetometer)
IC triple + IMU

Data consistency of differing sensors

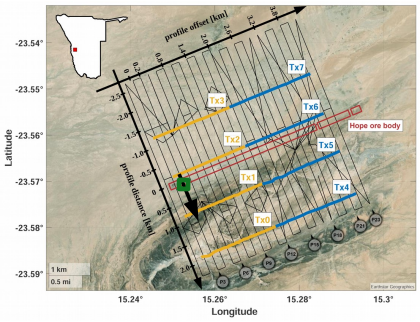

Fig. 5: Survey site at the Hope ore deposit (Namibia, 2021/2023). Shown are deployed EM transmitters (Tx0 - Tx7) and profile lines (P3 – P23) composed of several overlapping flight paths (black lines).

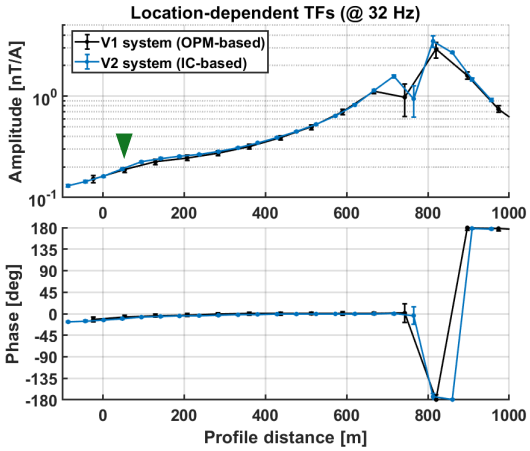

Fig. 6: Comparison of transfer function estimates. Depicted are TFs (in local total field direction) estimated using the OPM-based system (black lines) and one IC-based system (blue lines) along a profile line (P3) segment. Estimates for one active transmitter (Tx1) at 32 Hz are represented.

Data consistency of differing sensors

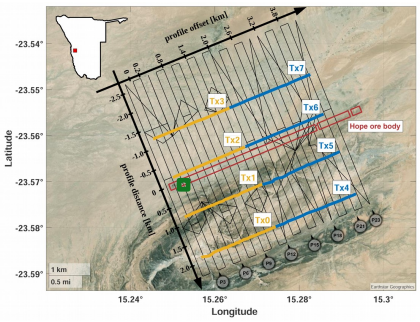

Fig. 5: Survey site at the Hope ore deposit (Namibia, 2021/2023). Shown are deployed EM transmitters (Tx0 - Tx7) and profile lines (P3 – P23) composed of several overlapping flight paths (black lines).

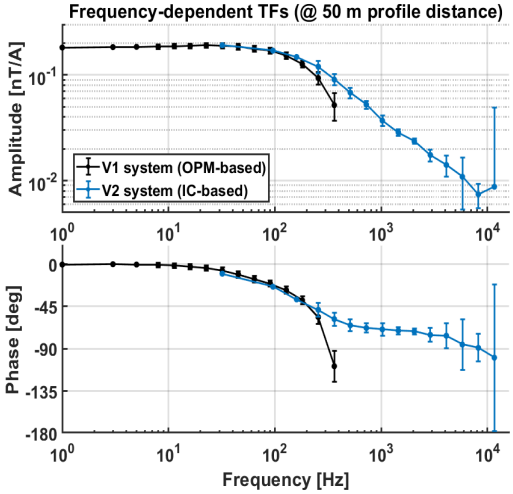

Fig. 7: Comparison of transfer function estimates. Depicted are TFs (in local total field direction) estimated using the OPM-based system (black lines) and one IC-based system (blue lines). Estimates at one location (50 m profile distance) along Profile 3 and for one active transmitter (Tx1) are shown.

System-related EM noise

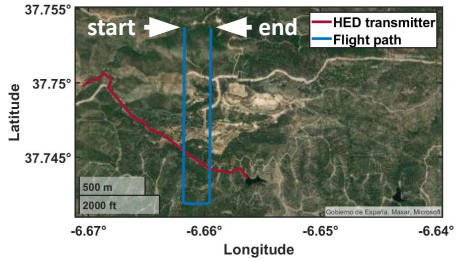

Fig. 8: Survey site near Huelva (Spain, 2022). The shown flight path was traversed employing different sensor platforms.

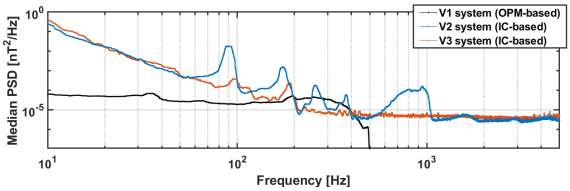

Fig. 9: Field spectra of different sensor platforms. Depicted are median PSD values of the magnetic field along local total field direction.

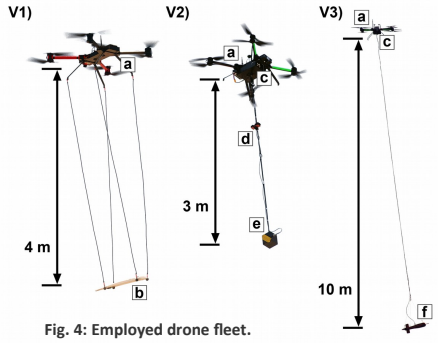

Fig. 4: Employed drone fleet.

System-related EM noise

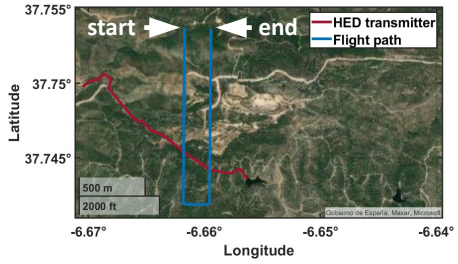

Fig. 8: Survey site near Huelva (Spain, 2022). The shown flight path was traversed employing different sensor platforms.

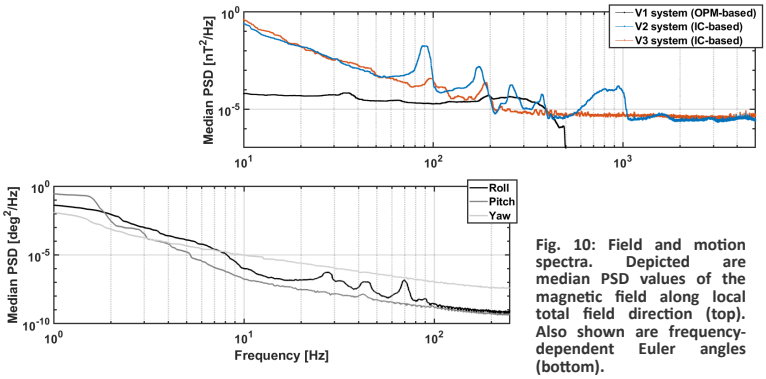

Fig. 10: Field and motion spectra. Depicted are median PSD values of the magnetic field along local total field direction (top). Also shown are frequency-dependent Euler angles (bottom).

System-related EM noise

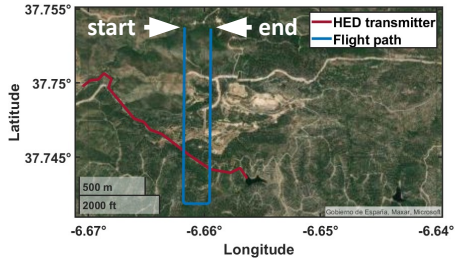

Fig. 8: Survey site near Huelva (Spain, 2022). The shown flight path was traversed employing different sensor platforms.

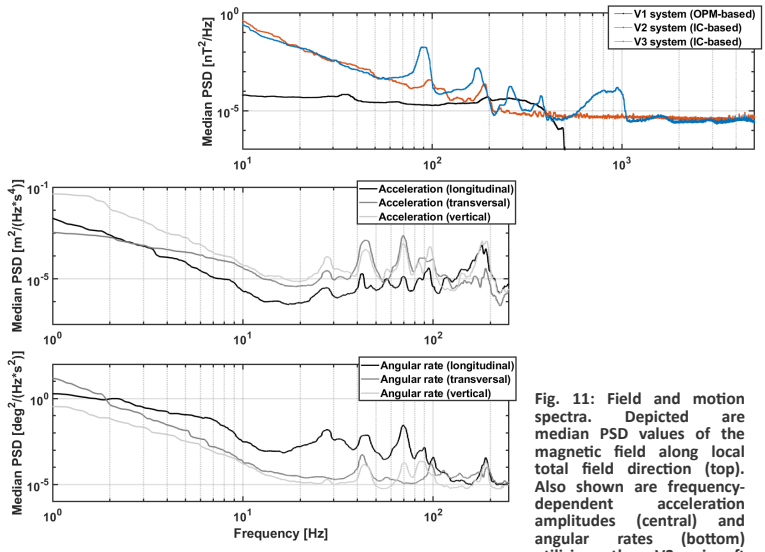

Fig. 11: Field and motion spectra. Depicted are median PSD values of the magnetic field along local total field direction (top). Also shown are frequency-dependent acceleration amplitudes (central) and angular rates (bottom) utilizing the V3 aircraft system.

System-related EM noise

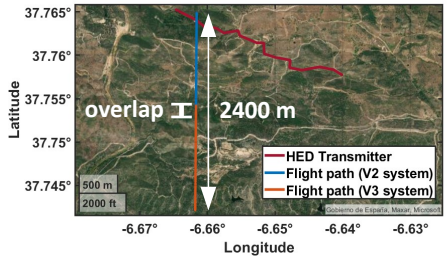

Fig. 12: Survey site near Huelva (Spain, 2022). Two overlapping flight paths employing differing aircraft systems are displayed.

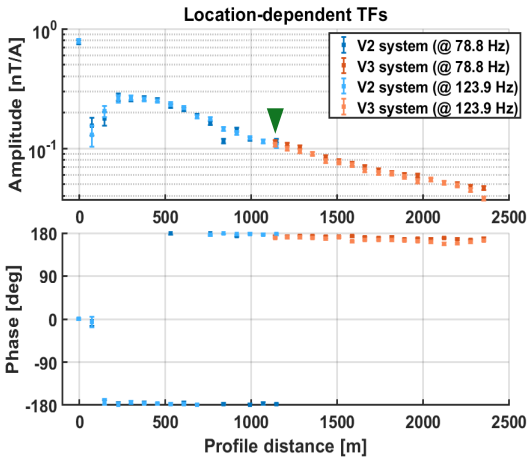

Fig. 13: Comparison of transfer function estimates. Depicted are non-binned TFs (in local total field direction) estimated for the V2 system (blue) and the V3 system (orange). Estimates along a profile line are shown.

System-related EM noise

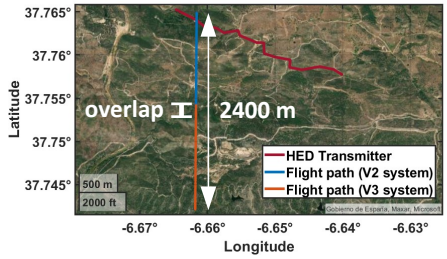

Fig. 12: Survey site near Huelva (Spain, 2022). Two overlapping flight paths employing differing aircraft systems are displayed.

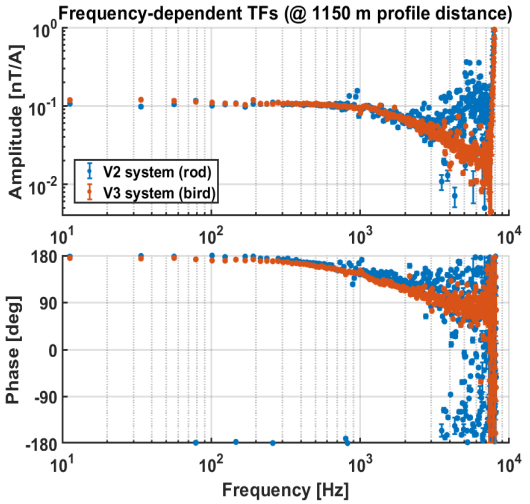

Fig. 14: Comparison of transfer function estimates. Depicted are non-binned TFs (in local total field direction) estimated for the V2 system (blue) and the V3 system (orange). Estimates at one location (1150 m distance to transmitter) are shown.

Conclusion & Outlook

- High data consistency among the utilized sensor platforms
- Severe influence of system-related EM noise (motion & emission)
  - < 400 Hz (motion predominant)
  - > 400 Hz (emission predominant)
- System-related advantages and disadvantages (flight velocity, field components measured, sensor sensitivity, noise behavior, ..)
- Operational capabilities for the semi-airborne EM method up to 6 kHz and 2.5 km transmitter distance
- Elaboration of suitable data weighting for inversion
- Reduction of the instrument load and optimization of the suspension
- Widening the scope of application for drone-based EM systems

WWU MÜNSTER

p. 18/18

Acknowledgments

Deep **E**lectromagnetic **S**ounding for **M**ineral **Ex**ploration

DESMEX

*We wish to express our gratitude for the financial support provided by the **Federal Ministry of Education and Research of Germany (BMBF)** as part of the DESMEX II initiative (project number: 03R130AN). Additionally, essential instrumentation was made possible through funding (grant reference: INST 211/864-1 FUGG) from the **German Research Association (DFG)**.*
*We would like to extend our appreciation to the members of the **DESMEX working group and to our project partners** for their insightful discussions regarding semi-airborne EM methodology and the realization of drone-based surveys.*
*Particular acknowledgment extends to **Terratec Geophysical Services** for facilitation and assistance in carrying out the campaign at the Hope Deposit in Namibia.*

Funding:

Federal Ministry of Education and Research

DFG Deutsche Forschungsgemeinschaft German Research Foundation

Project partners:

IAG Leibniz-Institut für Angewandte Geophysik

terratec Geophysical Services

Universität zu Köln

supracon

BGR Bundesanstalt für Geowissenschaften und Rohstoffe

iMAR NAVIGATION & CONTROL

Leibniz ipht Leibniz-Institut für Photonische Technologien

DMT

WWU MÜNSTER